Quaternary Research

doi:10.1017/qua.2020.10

Evidence for rapid paraglacial formation of rock glaciers in southern Norway from ^{10}Be surface-exposure dating

Henriette Linge[a]*, Atle Nesje[a], John A. Matthews[b], Derek Fabel[c], Sheng Xu[c]

[a]Department of Earth Science, University of Bergen and Bjerknes Centre for Climate Research, NO-5020, Bergen, Norway
[b]Department of Geography, College of Science, Swansea University, Swansea, SA2 8PP, Wales, UK
[c]AMS Laboratory, Scottish Universities Environmental Research Centre, East Kilbride G75 0QF, Scotland, UK
*Corresponding author at: E-mail address: henriette.linge@uib.no (H. Linge).

(Received August 31, 2019; Accepted January 31, 2020)

Abstract

We evaluate the timing and environmental controls on past rock-glacier activity at Øyberget, upper Ottadalen, southern Norway, using in situ ^{10}Be surface-exposure dating on (1) boulders belonging to relict rock-glacier lobes at c. 530 m asl, (2) bedrock and boulder surfaces at the Øyberget summit (c. 1200 m asl), and (3) bedrock at an up-valley site (c. 615 m asl). We find that the rock-glacier lobes became inactive around 11.1 ± 1.2 ka, coeval with the timing of summit deglaciation (11.2 ± 0.7 ka). This is slightly older than previously published Schmidt-hammer surface-exposure ages. The timing does not match known climatic conditions promoting rock-glacier formation in the early Holocene; hence we infer that lobe formation resulted from enhanced debris supply and burial of residual ice during and soon after deglaciation. The results demonstrate that rock glaciers may form over a relatively short period of time (hundreds rather than thousands of years) under non-permafrost conditions and possibly indicate a paraglacial type of process.

Keywords: Scandinavia; Norway; surface-exposure dating; cosmogenic nuclides; ^{10}Be; Schmidt-hammer; rock glacier; paraglacial landforms

INTRODUCTION

Recently, Knight and colleagues (2019) pointed out that rock glaciers remain a poorly understood geomorphic element of the landscape, at least in part because of their polygenetic origin in combination with the numerous ways they have been studied. The literature commonly refers to two main types of rock glaciers according to their mode of origin, glacier-derived and talus-derived (e.g., Barsch, 1996; Berthling, 2011), whereas landforms generated by a third mode, rock avalanche-derived rock glaciers (e.g., Whalley and Azizi, 2003), are largely ignored.

Talus-derived rock glaciers are considered indicative of periglacial conditions with permafrost (e.g., Barsch, 1996; Kääb, 2013). Ice formation within pre-existing talus accumulations, followed by downslope creep and deformation of the ice core and interstitial ice creates characteristic lobe shapes—talus-derived rock glaciers—that have high survival potential even after the internal ice disintegrates. Relict talus-derived rock glaciers are therefore a landform where reliable dating can give information about past regional climatic conditions. Dating of (active and relict) talus-derived rock glaciers ranges from relative dating techniques such as landform associations (e.g., Humlum, 2000), lichenometry (e.g., André, 1994), advance rates (e.g., Berthling and Etzelmüller, 2007), differential weathering as determined by photogrammetric measurements (e.g., Kellerer-Pirklbauer et al., 2008), and Schmidt-hammer methods (e.g., Shakesby et al., 2006) to numerical methods such as ^{14}C dating of organic material from the ice core (e.g., Haeberli et al., 1999; Konrad et al., 1999), ^{14}C dating of lake sediments affected by rock-glacier meltwater (Paasche et al., 2007), Schmidt-hammer calibrated-age dating (e.g., Matthews et al., 2013), surface-exposure dating of coarse debris using in situ cosmogenic ^{10}Be (e.g., Ballantyne et al., 2009; Hippolyte et al., 2009; Cossart et al., 2010), in situ ^{36}Cl (Çiner et al., 2017), and luminescence (optically stimulated luminescence and infrared stimulated luminescence) techniques on sand-rich horizons (Fuchs et al., 2013). Optically

Cite this article: Linge, H., Nesje, A., Matthews, J. A., Fabel, D., Xu, S. 2020. Evidence for rapid paraglacial formation of rock glaciers in southern Norway from ^{10}Be surface-exposure dating. *Quaternary Research* 97, 55–70. https://doi.org/10.1017/qua.2020.10

stimulated luminescence dating of rock surfaces (e.g., Sohbati et al., 2012) does not appear to have been applied to talus-derived rock glaciers yet.

Ottadalen in southern Norway (Fig. 1A, B) is located inside the margin of the Younger Dryas (YD) ice sheet. Lobate, coarse rock-debris accumulations are found in Øybergsurdi beneath the south-facing wall of Øyberget (Fig. 1C, D) in upper Ottadalen. These features are not included in the regional rock-glacier inventory presented by Lilleøren and Etzelmüller (2011). However, Matthews and colleagues (2013) discussed whether these landforms are relict talus-derived rock glaciers or rock-slope failure accumulations and concluded that their morphology is clearly consistent with the former. This study builds on their interpretation.

Three lobes were dated by Matthews and colleagues (2013) using Schmidt-hammer surface-exposure dating, yielding 10,340 ± 1280, 9920 ± 1385, and 8965 ± 1700 years for Lobes 1, 2, and 3 (Fig. 1D), respectively. A Schmidt hammer measures the surface hardness or compressive strength of a rock surface via the extent of rebound (R) from when the hammer's spring-controlled plunger hits the surface. Schmidt-hammer surface-exposure dating uses R values from surfaces of known age for age calibration of R values from surfaces of unknown age (e.g., Shakesby et al., 2011; Wilson and Matthews, 2016). The early Holocene ages, however, are inconsistent with the absence of a permafrost climatic regime at the time. Two scenarios were suggested to explain the landform ages: (1) rapid early-Holocene paraglacial formation where residual glacial ice was buried by debris, or (2) a slower formation under permafrost conditions during an earlier interstadial with subsequent preservation beneath cold-based ice. In this study, we apply in situ cosmogenic ^{10}Be surface-exposure dating to test these two scenarios. ^{10}Be is produced in quartz exposed at the Earth's surface by interaction between the mineral and secondary cosmic-ray particles (Gosse and Phillips, 2001), and the concentration of ^{10}Be in a rock surface thus allows calculation of the duration of exposure.

Several studies have compared results obtained using the two methods (e.g., Engel, 2007; Sánchez et al., 2009; Winkler, 2009; Wilson et al. 2019a; 2019b). Although both dating approaches rely on subaerial exposure, their measures of time rely on fundamentally different parameters affecting the rock surfaces (i.e., rate of chemical weathering versus production of in situ cosmogenic nuclides). This paper therefore makes a general contribution, not only to understanding the dating and formation of rock glaciers, but also to the methodology of two geochronological methods.

REGIONAL SETTING

Physical and geological characteristics of the region

Ottadalen in southern Norway (Fig. 1A, B) extends from the town of Otta in the east towards the water divide at Strynefjellet (S in Fig. 1B) in the west. The easternmost outlet glaciers of Jostedalsbreen (J in Fig. 1B), the largest glacier on continental Europe today (487 km^2), are located 25 km west of Øyberget.

Ottadalen is the largest tributary valley to Gudbrandsdalen valley (Fig. 1B), and its valley floor increases from 380 m asl in the east to 450 m asl in the west. The valley has a typical U-shape with steep valley sides and over-deepened troughs. The study area (Fig. 1C, D) consists predominantly of dioritic to granitic gneisses of Precambrian age (Lutro and Tveten, 1996) that dip 60° north. Boulders in the rock-glacier study sites are of local origin from the Øyberget cliff face and are mainly composed of a distinctive banded gneiss with white bands of quartz-feldspar, pink bands of potassium-feldspar, and gray bands of biotite-mica.

Prior ^{10}Be surface-exposure ages in the vicinity have been reported by Goehring and colleagues (2008) from boulders along an altitudinal transect from 1086 to 1617 m asl at Blåhø in lower Ottadalen, about 60 km east of Øyberget. They found that boulders on striated bedrock yield ^{10}Be ages of 10–12 ka, boulders on exposed bedrock or thin till give ^{10}Be ages of 15–30 ka, and one boulder from the summit blockfield gave a ^{10}Be age of 25 ka. A progressive divergence between ^{10}Be surface-exposure ages of bedrock and boulders (Supplementary data in Goehring et al., 2008) with increasing elevation was interpreted as reflecting cold-based, low-erosive glacier cover at higher elevations. The minimal divergence below 1300 m asl was interpreted as confirming rapid deglaciation after 15 ka. Recently, Marr and colleagues (2019) added cosmogenic ^{10}Be surface-exposure ages of 21 ka (boulder) and 46 ka (bedrock) to the Blåhø dataset. In addition, they report ^{10}Be surface-exposure ages of 13 ka (bedrock) from Dalsnibba (1476 m asl), 45 km northwest of Øyberget. Again, using cosmogenic ^{10}Be surface-exposure dating, Andersen and colleagues (2019) found that boulders > 1600 m asl on the Reinheimen plateau, 20–40 km east of Øyberget, give a deglaciation age around 10.5 ka (global calibration dataset, Lal-Stone time-independent scaling scheme).

Additional evidence of former cold-based, low-erosive ice sheets is found at multiple sites in the Gudbrandsdal region displaying water-deposited sub-till sediments (i.e., sediments overridden by later glaciation and hence overlain by till) of interstadial origin (see Bergersen and Garnes, 1983, and references therein). In upper Ottadalen, examples of such sites are located 10 km west and 21 km east of Øyberget. The overlying tills have been correlated and used to reconstruct changes in ice-movement directions during the last glaciation in Ottadalen (Bergersen and Garnes, 1983). Four phases are defined from the stratigraphy: (i) a glacial inception phase with down-valley (eastwards) ice flow, (ii) an early regional phase with the ice divide (culmination zone) located parallel to the regional water divide across upper Ottadalen (no lateral flow), (iii) an inland ice phase with across-valley ice flow towards the northwest, and (iv) a late regional phase with across-valley ice flow towards the northeast. Without numerical chronology of these phases, it is impossible to rule out preservation of pre-last glacial maximum (LGM) deposits.

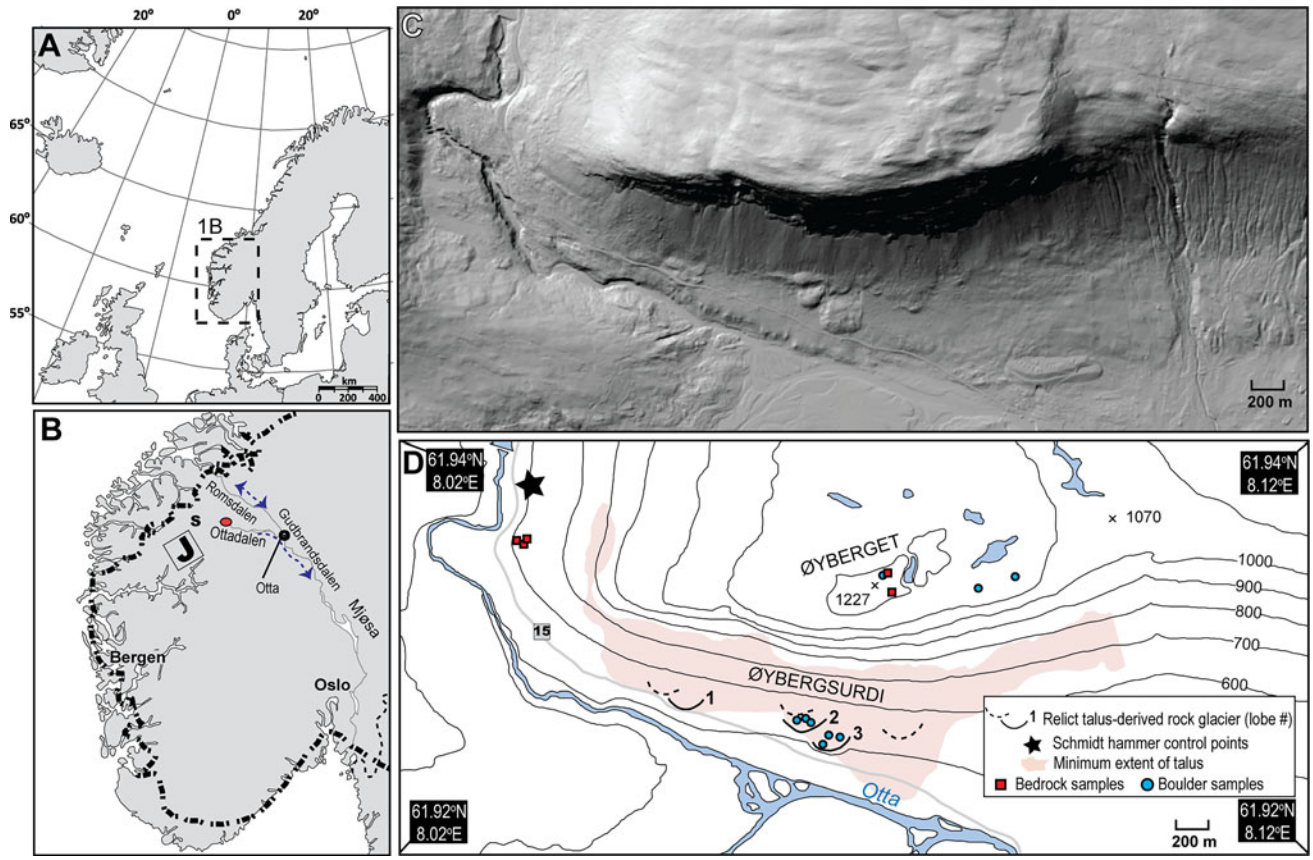

Figure 1. (color online) (A) Map of the North Atlantic, the rectangle (dashed line) outlines southern Norway shown in (B). (B) The broken line shows the approximate position of the Younger Dryas ice-sheet margin in southern Norway (modified from Andersen et al., 1995). The oval marks the location of the study site, west of the town of Otta and east of Strynefjellet (S). J indicates the approximate location of the glacier Jostedalsbreen. The drainage direction (arrows) of river courses go through the valleys Romsdalen, Ottadalen, Gudbrandsdalen, and via lake Mjøsa to the sea southeast of Oslo. (C) Digital elevation model of the uppermost part of Ottadalen valley showing lobes along the Øybergsurdi talus slope (https://hoydedata.no/LaserInnsyn/). (D) Simplified topographic map of the uppermost part of Ottadalen valley showing the minimum extent of the Øybergsurdi talus (shaded area) as mapped from aerial photos. Locations of the boulder samples (circles) and bedrock samples (squares) are shown for the four sites Summit, Up-valley, Lobe 2, and Lobe 3 investigated in this study. The star indicates the location of the control points used in the Schmidt-hammer dating study of Matthews et al. (2013), in which Lobes 1–3 were first dated.

Upper Ottadalen was ice covered during the YD stadial (12.8–11.7 ka) when the margin of the Scandinavian Ice Sheet (SIS) was located in the fjord heads to the west. Regional ice-sheet reconstructions by Hughes and colleagues (2016) and Stroeven and colleagues (2016) depict how the SIS margin retreated eastwards to expose the field area between 11 and 10 ka. Outlet glaciers of Jostedalsbreen, the plateau glacier to the west, formed two prominent marginal moraines at 10.1 and 9.7 cal ka BP (see Nesje [2009] and references therein). Matthews and colleagues (2013) assumed that upper Ottadalen became ice free immediately after the Erdalen Event (10.1–9.7 cal ka BP, Dahl et al., 2002; i.e., at c. 9.7 cal ka BP).

Reconstructions of the total glacio-isostatic rebound in Fennoscandia indicate that upper Ottadalen has experienced a total uplift in the order of 125 m since 12 ka (e.g., Lysså et al., 2008; Vorren et al. 2008, p. 541), of which half or perhaps two-thirds occurred prior to 8 ka. The present-day uplift rate is 2–3 mm yr^{-1} (Dehls et al., 2000). Upper Ottadalen has been pine dominated since shortly after the deglaciation (Paus, 2010; Paus and Haugland, 2017), and pine grew at least up to 1270 m asl (present elevation) between 9.8 and 7.7 cal ka BP (Paus and Haugland, 2017; Paus et al. 2019). The present-day pine-tree limit in the region is about 950 m asl.

Matthews and colleagues (2013) used temperature and precipitation data from the closest meteorological station to estimate the mean annual air temperature (MAAT) and mean annual precipitation at the elevation of the relict rock-glacier lobes (c. 520 m asl, Supplementary Table 1). The climatic normal period 1961–1990 yielded a MAAT of 1.6° C and mean annual precipitation of 295 mm (Matthews et al., 2013).

Information about annual snow cover is not available as measurement records, but modelled data is available from 1 September 1957, until today via the online resource, seNorge.no (http://www.senorge.no). Weather and snow data with a spatial and temporal resolution of 1 km and 24 hours, respectively, is displayed on topographic maps. Weather data is calculated via spatial interpolation of point

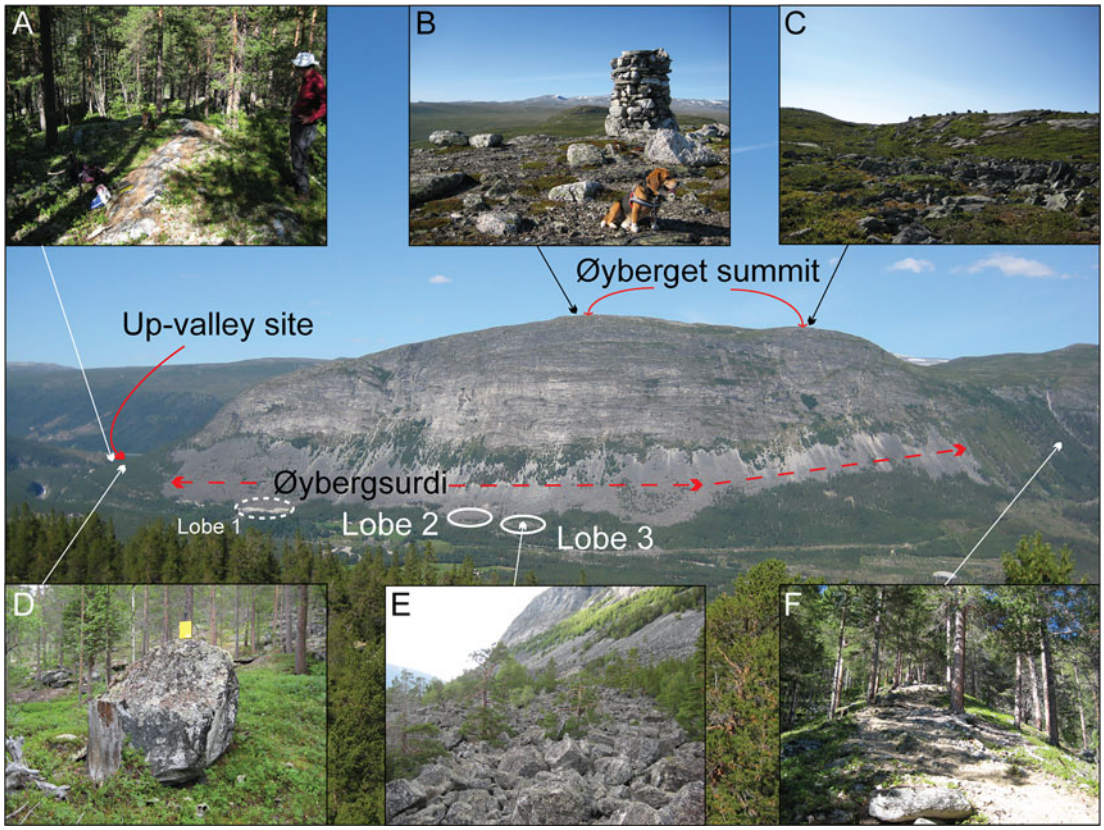

Figure 2. (color online) Overview (main photo) of Øyberget from the south, showing the locations of the sites in this study: Summit, Up-valley, Lobe 2, and Lobe 3. A clear transition from the steep cliff face to the talus slope is evident at approximately 800 m asl. Bare bedrock is exposed at the Up-valley site (A) and at the Summit (B, C) where glacially transported boulders are common. Boulders at the Up-valley site may originate both from glacial transport (boulder in the foreground, D) and rock fall activity (boulders in the background, D). The lower part of the talus slope has multiple lobate-shaped landforms, where the most prominent are Lobes 1–3. The uneven surface of Lobe 3 is shown in (E), and the slightly higher Lobe 2 can be seen in the background (photo taken from boulder F towards west, see Fig. 3). The mountain slope east (down valley) of the slope has a thick till cover (F), in sharp contrast to the Up-valley and Summit sites.

observations, while snow data are simulated with snow models using the weather data. Although it is uncertain how well the modelled snow data depict the actual conditions at the rock-glacier site, comparison of measured and modelled data for the nearest weather station (Gjeilo-i-Skjåk, 378 m asl) suggest that the snow data are likely to be representative (Supplementary Table 1).

The study area lies below the regional lower limit of discontinuous permafrost. In southern Norway the limit is around 1500 m asl, corresponding to a mean annual temperature of about 3°C (Lilleøren et al., 2012). Data from three boreholes 60 km east of the study area show permafrost at 1560 m asl but not at 1450 m or below (NORPERM, 2018; http://geo.ngu.no/kart/permafrost/).

Location and characteristics of the sampling sites

Application of in situ cosmogenic ^{10}Be surface-exposure dating, not only to determine the age of relict rock glaciers but also to determine surface-exposure ages of other landform surfaces, is crucial for determining the timing of rock-glacier formation. Samples for in situ ^{10}Be dating in this study were collected from four locations: the Øyberget summit, the up-valley site, Øybergsurdi lobe 2, and Øybergsurdi lobe 3 (Fig. 2). These will be referred to as "Summit," "Up-valley," "Lobe 2," and "Lobe 3" for simplicity. Lobe 1 was not visited because of ongoing quarrying.

The Summit (> 1200 m asl) has a discontinuous to thin (< 0.5 m) cover of till and numerous glacially transported gneiss boulders (Fig. 2B, C). The exposed bedrock at the summit area exhibits polished quartz-rich veins and smooth glacially eroded surfaces with plucked edges. Five samples were collected and processed from the summit area (Fig. 3A–E, Table 1); of these, two were from bedrock (Fig. 3A–C) and three were from boulders (Fig. 3A, D, E).

The Up-valley site (Fig. 1, 2) is located west of the Øybergsurdi talus slope and about 2 km up-valley from Lobe 2. Bedrock exposures here consist of smooth glacially eroded surfaces (Fig. 2A) and polished quartz-rich lenses. Most boulders here are situated close to the slope, indicative of a clear rockfall origin (Fig. 2D), and the very few convincing glacially deposited boulders have unsuitable size and/or geometry for surface-exposure dating. Other boulders occur in groups beyond the extent of the obvious talus deposits;

Figure 3. (color online) Rock surfaces sampled (marked with a star) for ^{10}Be surface-exposure dating at the Summit (A–E), Up-valley (F–G), Lobe 2 (H–J) and Lobe 3 (K–N). (A) Sample ØYB 1301 from bedrock (open notebook for scale) and sample ØYB 1302 from a boulder (boulder-s1) surface 60 cm above the bedrock. (B) Sample ØYB 1303 from an exposed bedrock surface (rucksack in the background for scale), 56 m from sample ØYB 1301. (C) A close-up of the sampled vein in (B). (D) Sample ØYB 1304 from the surface of the boulder-s2 resting on bedrock (standing hammer for scale). (E) Sample ØYB 1305 from the surface of boulder-s3 resting in a bedrock niche (standing hammer for scale). (F) Samples ØYB 1306 and ØYB 1307 from exposed bedrock surfaces, less than 3 m apart, at the Up-valley site. (G) Sample ØYB1308 from bedrock, approximately 40 m north of surfaces shown in (F). (H) Sample ØYB 1201 from the sub-horizontal surface of boulder-2a on Lobe 2. Sitting beagle (41 cm at the withers) for scale, c. 50 cm tall. (I) Sample ØYB 1202 from the horizontal surface of boulder-2b (Lobe 2) to the right of the pine tree (rucksack leaning towards the tree trunk for scale). The pine tree in the background is the same as in Figure 3H here and Figure 4a of Matthews et al. (2013). (J) Sample ØYB 1203 from the small flat top surface of pointy boulder-2c (standing hammer for scale). The boulder is located closer to the front of Lobe 2 than boulders-2a and -2b. (K) Sample ØYB 1204 from a weathered and detached, but still in situ, piece of the top surface of boulder-3a, and sample ØYB 1205 from a quartz-rich knob from the highest part of the surface of boulder-3a. Eastern part of Lobe 3, sitting beagle (c. 50 cm tall) for scale. (L) Sample ØYB 1206 from boulder-3b in the middle part of the uneven surface of Lobe 3 with 25-cm-long orange angle square ruler for scale. (M) Samples ØYB 1207 and ØYB 1208 from the surface of boulder-3c, situated close to boulder-3b. A 30-cm-long tool bag is barely visible as a scale. (N) Sample ØYB 1309 from a quartz vein exposed at the top point of boulder-3d, situated close to the steep front of Lobe 3. Tall person for scale.

Table 1. Summary of field data for samples for ^{10}Be surface-exposure dating.

Sample ID	Elevation (m asl)	Lithology	Surface type (boulder L×W×H in m)	Sample information	Latitude (°N)	Longitude (°E)	Shielding factor[a]	Thickness (cm)
Summit (Figures 3A–E)								
ØYB 1301	1225	Biotite gneiss	Bedrock, weathered	Semi-detached piece	61.92930	8.07355	0.9999	3.0
ØYB 1302	1225	Gray gneiss	Boulder s1 (1.2×0.75×0.6)	Several pieces	61.92930	8.07355	0.9999	2.0
ØYB 1303	1221	Pegmatite	Bedrock, polished	Quartz-rich vein, one piece	61.92908	8.07451	0.9999	2.5
ØYB 1304	1191	Biotite gneiss	Boulder s2 (1×1×0.75)	One piece	61.92949	8.08535	0.9999	1.5
ØYB 1305	1175	Gray gneiss	Boulder s3 (1.2×1×0.9)	Several pieces	61.93031	8.08845	0.9996	1.0
Up-valley site (Figures 3F, G)								
ØYB 1306	615	Pink gneiss	Bedrock, exposed	Semi-detached piece	61.92940	8.03356	0.9879	1.5
ØYB 1307	615	Pink biotite gneiss	Bedrock with moss	Semi-detached piece	61.92934	8.03375	0.9879	10.0
ØYB 1308	617	Gray gneiss	Bedrock, exposed	Detached piece by root	61.92968	8.03401	0.9879	7.0
Lobe 2 (Figures 3H–J)								
ØYB 1201	540	Banded gneiss	Boulder 2a (4×3×1)	2 pieces, semi-detached	61.92157	8.06649	0.9389	3.0
ØYB 1202	542	Banded gneiss	Boulder 2b (1.5×1×2)	6 pieces chiselled off	61.92166	8.06673	0.9358	2.0
ØYB 1203	538	Banded gneiss	Boulder 2c (2.5×1.5×1.2)	Thick piece from cracked top	61.92149	8.06693	0.9321	6.0
Lobe 3 (Figures 3K–N)								
ØYB 1204	517	Banded gneiss	Boulder 3a (5×2×2)	Detached piece, weathered	61.92086	8.07121	0.9551	4.0
ØYB 1205	517	Banded gneiss	Boulder 3a (5×2×2)	Quartz-rich piece	61.92086	8.07121	0.9551	3.5
ØYB 1206	528	Banded gneiss	Boulder 3b (3.5×1.5×0.5)	Piece collected along crack	61.92128	8.07002	0.9401	1.0
ØYB 1207	528	Banded gneiss	Boulder 3c (6×3×2)	Small pieces from top surface	61.92127	8.06968	0.9401	3.0
ØYB 1208	528	Banded gneiss	Boulder 3c (6×3×2)	One piece from top surface	61.92127	8.06968	0.9401	3.8
ØYB 1309	515	Quartz	Boulder 3d (1.5×1×1.6)	Quartz vein at pointy top	61.92059	8.06974	0.9620	1.5

[a]Geometric shielding correction was computed after Dunne et al. (1999).

these boulder accumulations are situated on exposed bedrock and in depressions between exposed bedrock. Plucking and transport by either glaciers or meltwater could explain these accumulations. Three bedrock samples (Fig. 3F, G) were collected and processed from the Up-valley site (Table 1).

The Øybergsurdi talus slope, beneath the Øyberget summit (1227 m asl) (Fig. 1C, D, 2) covers more than 1 km^2 and has several lobe-shaped features along its lower part. The most pronounced lobes are found at an elevation of 510–540 m asl, and they are up to 200 m wide and 200 m long. The lobes have steep fronts, uneven and low-angle surfaces, and sharp transitions to the talus slope behind them (Fig. 2E). The base of the talus slope and inter-lobe area are forested; the vegetation on the lobes themselves is very sparse except for the occasional pine. Mosses and heath species are often confined to small depressions on the boulder surfaces, and lichens are typically present on all exposed rock surfaces. The boulders comprising the open-work lobes are large, typically 1–3 m long on their longest axis. Traversing these lobes is like climbing a coarse, subhorizontal scree deposit; individual boulders often protrude 1–2 m above their base or surrounding ground, and they are typically 0.5–2 m apart. Most boulders are firmly stuck in the landform, but some boulders are loose. Few large boulder surfaces have smaller, very angular boulders on top, suggesting rock fall deposition. No glacially transported (perched/erratic) boulders were observed. All boulder surfaces selected for sampling were at least 1 m above the boulder's base and were horizontal to subhorizontal, and shielding from surrounding boulders was less than the topographic horizon. Three samples were collected and processed from boulder surfaces on Lobe 2 (Fig. 3H–J, Table 1), and six were collected and processed from boulder surfaces on Lobe 3 (Fig. 3K–N, Table 1).

The valley slope (Fig. 2F) east of the Øybergsurdi talus slope has a thick (> 10 m) till cover up to about 800 m asl (i.e., no bedrock exposures were observed in ravines, only in parts of the stream, and no material was collected for dating). It stands, however, in sharp contrast to the exposed

bedrock at the Up-valley site and Summit area, the Øybergsurdi talus slope, and the open-work Lobes 2 and 3.

MATERIALS AND METHODS

Field sampling

In the field, it is crucial to collect samples that are representative of the geological problems and/or hypotheses being investigated or tested. This seems straightforward, but it does not always turn out to be so. ^{10}Be is produced within quartz through spallation of oxygen and muon-induced reactions (Gosse and Phillips, 2001), and its concentration is in theory a measure of how long a surface has been exposed to secondary cosmic radiation. That is, it indicates whether the rock surface has had a single-stage, continuous exposure history in the same position. In the case of pre-exposure, temporal cover, and geometric or elevation change, the concentration represents a more complex history (e.g., Ivy-Ochs et al., 2007).

Gneiss surfaces were sampled using a hammer and chisel for in situ cosmogenic ^{10}Be surface-exposure dating of material from three different settings: glacially eroded bedrock, glacially transported boulders, and rock-glacier boulders. Sample locations and elevations were recorded in the field with a hand-held GPS (Garmin 60SCx) and later confirmed from a digital elevation model (Høydedata, 2018; https://hoydedata.no/LaserInnsyn/). Figure 3 shows the sampled surfaces from the Summit site (Fig. 3 A–E), the Up-valley site (Fig. 3F, G), and Lobes 2 and 3 (Fig. 3H–N). Topographic shielding was determined for each surface based on clinometer readings to the horizon. Sample thickness was measured in the field and re-checked prior to crushing. Observations on weathering, erosion, and snow shielding were noted. Table 1 summarizes the field data relevant for calculating ^{10}Be concentrations.

Sample preparation

Rock samples were processed at the Department of Earth Science (GEO), University of Bergen (UiB), using standard mineral-separation techniques (Kohl and Nishiizumi, 1992) on the 0.25–0.5 mm fraction. Quartz purity was assessed by ICP-OES measurement of aluminum; concentrations less than 100 ppm were desired for optimal column chemistry yields. Preparation of samples from clean quartz to targets for accelerator mass spectrometry (AMS) measurement of ^{10}Be/^{9}Be was done according to procedures modified from Child and colleagues (2000). Beryllium extraction was done at GEO, UiB, and Be targets for AMS analysis were prepared at the Scottish Universities Environmental Research Centre (SUERC) Cosmogenic Isotope Laboratory. ^{10}Be/^{9}Be ratios were measured on the 5 MV AMS at SUERC (Xu et al., 2010) in 2015. The average process blank (^{10}Be/^{9}Be $= 3.18 \pm 0.75 \times 10^{-15}$, $n = 3$) was subtracted from sample ^{10}Be/^{9}Be values to account for background levels of ^{10}Be.

Table 2. Relevant correction factors for the sites in upper Ottadalen and the approximate (exposure-time dependent) percent increase in ^{10}Be surface-exposure age when accounted for.

Site	Erosion[a]	Uplift[b]	Snow[c]	Forest[d]
Summit	0.32–0.48%	3.1–4.1%	2.0%	--
Up-valley	0.33–0.37%	3.4–4.0%	1.5%	2.25%
Lobe 2 and 3	0.36–0.47%	4.0–4.6%	1.5%	--

[a]Erosion by chemical weathering and removal of grains is in the order of 0.48 mm ka^{-1} based on observed relief (4–5 mm) of polished quartz veins near the Up-valley site.
[b]Based on uplift data compiled by Lysså et al. (2008).
[c]Based on monthly snow depth data calculated from modelled daily snow thickness for years 1958–2017 (SeNorge, 2018) and calculated using a snow density of 0.2 g cm^{-3} and an attenuation length in snow of 160 g cm^{-2} (see references in Gosse and Phillips, 2001).
[d]Reduction in ^{10}Be production rate due to shielding by forest is adapted from Plug et al. (2007).

Calculation of ^{10}Be surface-exposure ages

When calculating in situ ^{10}Be ages, certain assumptions were made with regard to the erosion and exposure history of the rock surfaces. Relevant correction factors for erosion, uplift (glacio-isostatic rebound), snow cover, and forest are presented in Table 2. Table 3 presents laboratory data, calculated ^{10}Be concentrations (2.6%–6.0% range in analytical 1σ errors), and ^{10}Be surface-exposure ages. Ages are obtained using the online exposure age calculator formerly known as the CRONUS-Earth online exposure age calculator, version 3 (Balco, 2017), available at http://hess.ess.washington.edu/math/v3/v3_age_in.html. We apply the Scandinavian calibration set of Stroeven and colleagues (2015) (18 samples from 4 sites, available at http://calibration.ice-d.org/cds/2), and the calculator computes reference production rates (via spallation) and exposure ages according to the Lm scaling scheme (Balco et al., 2008) where the latitude-altitude-based scaling factors of Lal (1991) are modified to account for geomagnetic field variability (Lifton, 2016). The Scandinavian ^{10}Be production rate (Stroeven et al., 2015) has a reference sea-level high-latitude ^{10}Be production rate of 4.13 ± 0.11 atoms g^{-1} yr^{-1} (Lm scaling).

RESULTS

^{10}Be surface-exposure ages

The calculated in situ ^{10}Be ages obtained for the 17 samples span from 8.9 ± 0.3 to 11.0 ± 0.5 ka (1σ analytical uncertainty) and show close to insignificant variation within and between the individual sites: Summit, Up-valley, Lobe 2, and Lobe 3 (Fig. 4, Table 3).

For the Summit site (1225–1175 m asl), ^{10}Be surface-exposure ages (8.9 ± 0.3 to 11.0 ± 0.3 ka) overlap within 2σ, except for youngest age (Fig. 4, Table 3). The agreement between bedrock and boulders implies that both surface types

Table 3. Laboratory data calculated and corrected ^{10}Be surface-exposure ages for the samples from upper Ottadalen, southern Norway.

Sample ID[1]	Elevation (m asl)	Quartz[2] (g)	Be carrier[3] (g)	^{10}Be/^{9}Be[4,5] ($\times10^{-15}$)	^{10}Be conc.[6] (10^4 at g^{-1} SiO_2)	^{10}Be surface exposure age[7] (ka)	
						Calculated ages[8]	*Corrected ages*[9]
Summit site (n = 5)							
ØYB 1301 (bedrock)	1225	26.3629	0.2334	219.85 ± 6.03	12.79 ± 0.37	*8.89 ± (0.26) 0.59	*9.39 ± (0.27) 0.62
ØYB 1302 (boulder s1)	1225	21.2583	0.2292	223.79 ± 5.82	15.87 ± 0.44	10.95 ± (0.30) 0.72	11.68 ± (0.32) 0.77
ØYB 1303 (bedrock)	1221	26.4254	0.2309	255.38 ± 6.32	14.71 ± 0.38	10.22 ± (0.27) 0.66	10.84 ± (0.28) 0.71
ØYB 1304 (boulder s2)	1191	21.5853	0.2329	214.17 ± 5.40	15.19 ± 0.41	10.73 ± (0.29) 0.70	11.45 ± (0.31) 0.75
ØYB 1305 (boulder s3)	1175	24.6504	0.2309	235.06 ± 8.24	14.49 ± 0.53	10.33 ± (0.38) 0.72	10.97 ± (0.40) 0.77
*Arithmetic average age ± one standard deviation (omitting *):*						*10.56 ± 0.34*	*11.24 ± 0.39*
Arithmetic average age ± propagated (analytic) systematic 1σ uncert. (omitting *):						***10.56 ± (0.62) 1.40***	***11.24 ± (0.67) 1.50***
Up-valley site (n = 3)							
ØYB 1306 (bedrock)	615	23.0704	0.2324	126.93 ± 3.93	8.32 ± 0.28	9.76 ± (0.33) 0.67	10.55 ± (0.36) 0.73
ØYB 1307 (bedrock)	615	20.2292	0.2316	100.10 ± 5.62	7.40 ± 0.44	9.30 ± (0.56) 0.79	9.99 ± (0.60) 0.85
ØYB 1308 (bedrock)	617	20.3169	0.2337	100.38 ± 3.99	7.46 ± 0.33	9.13 ± (0.40) 0.68	9.81 ± (0.43) 0.73
Arithmetic average age ± one standard deviation:						*9.40 ± 0.33*	*10.12 ± 0.38*
Arithmetic average age ± propagated (analytic) systematic 1σ uncert.:						***9.40 ± (0.77) 1.24***	***10.12 ± (0.83) 1.34***
Lobe 2 (n = 3)							
ØYB 1201 (boulder 2a)	540	21.2492	0.2299	113.68 ± 3.55	7.98 ± 0.28	10.67 ± (0.37) 0.74	11.38 ± (0.40) 0.79
ØYB 1202 (boulder 2b)	542	21.7202	0.2310	112.87 ± 3.98	7.78 ± 0.30	10.34 ± (0.40) 0.74	10.97 ± (0.43) 0.78
ØYB 1203 (boulder 2c)	538	22.6147	0.2300	116.29 ± 4.17	7.67 ± 0.30	10.61 ± (0.42) 0.76	11.32 ± (0.45) 0.81
Arithmetic average age ± one standard deviation:						*10.54 ± 0.18*	*11.22 ± 0.22*
Arithmetic average age ± propagated (analytic) systematic 1σ uncert.:						***10.54 ± (0.69) 1.29***	***11.22 ± (0.74) 1.38***
Lobe 3 (n = 6)							
ØYB 1204 (boulder 3a)	517	23.9770	0.2284	114.77 ± 5.10	7.09 ± 0.34	9.60 ± (0.46) 0.73	10.18 ± (0.49) 0.78
ØYB 1205 (boulder 3a)	517	21.6581	0.2332	110.29 ± 5.34	7.69 ± 0.40	10.37 ± (0.54) 0.82	11.01 ± (0.57) 0.87
ØYB 1206 (boulder 3b)	528	20.4203	0.2310	106.33 ± 4.32	7.75 ± 0.34	10.30 ± (0.46) 0.77	10.93 ± (0.49) 0.82
ØYB 1207 (boulder 3c)	528	24.3303	0.2333	130.56 ± 5.83	8.15 ± 0.39	11.00 ± (0.52) 0.84	11.74 ± (0.56) 0.90
ØYB 1208 (boulder 3c)	528	21.8031	0.2305	115.42 ± 3.90	7.92 ± 0.30	10.75 ± (0.40) 0.76	11.48 ± (0.43) 0.81
ØYB 1309 (boulder 3d)	515	22.2972	0.2307	121.28 ± 3.62	8.15 ± 0.27	10.76 ± (0.36) 0.73	11.43 ± (0.38) 0.78
Arithmetic average age ± one standard deviation:						*10.47 ± 0.50*	*11.13 ± 0.56*
Arithmetic average age ± propagated (analytic) systematic 1σ uncert.:						***10.47 ± (1.13) 1.90***	***11.13 ± (1.21) 2.03***

[1]All AMS targets were prepared and measured at SUERC.
[2]A density value of 2.65 g cm^{-3} is used for all samples.
[3]Be carrier concentration: 998.9 ± 3.6 µg/g.
[4,10]^{10}Be/^{9}Be isotope ratios are normalised to the NIST SRM Be standard assuming a ^{10}Be/^{9}Be nominal value of 3.06×10^{-11} (i.e., AMS standard NIST_30600 in the online calculator, see note 7). AMS data and data derived from this are given with 1σ uncertainties.
[5]A procedural ^{10}Be/^{9}Be blank value of $3.253 \pm 0.771\times10^{-15}$ (n = 3) is used to correct for background.
[6]Propagated uncertainties include error in the blank and counting statistics.
[7,10]^{10}Be surface exposure ages were calculated with "the online calculator formerly known as the CRONUS-Earth online calculator" (Balco et al., 2008) version 3, the Lm scaling model, and the Scandinavian ^{10}Be production calibration dataset (Stroeven et al., 2015). Analytical uncertainties are given in parentheses; systematic uncertainties (after parentheses) include the ^{10}Be production rate and ^{10}Be decay constant uncertainties. Arithmetic average ages are reported with (1) one standard deviation (1 SD) in parentheses for internal/^{10}Be data comparison, and (2) propagated 1-sigma (analytic) systematic uncertainties for comparison with non-^{10}Be data.
[8]Calculated ages: assuming no atmospheric pressure anomalies (std model), no significant erosion during exposure ($\epsilon = 0$ mm ka^{-1}), no prior exposure, no glacio-isostatic rebound, and no local temporal shielding (e.g., snow, sediment, soil, vegetation).
[9]Corrected ages (see Table 2 for details) assuming no atmospheric pressure anomalies (std model), an erosion rate of 0.48 mm ka^{-1} for gneiss surfaces, no prior exposure, 3.1%–4.6% increase in ^{10}Be concentration to compensate for glacial rebound, 2% reduction in ^{10}Be production for the forested Up-valley site, and moderate snow shielding (1.5% reduction in ^{10}Be production for Up-valley and Lobe sites, and 2.0% for the Summit site).

were sufficiently eroded by glacial processes that nuclide inheritance is not an issue, and that the surface-exposure ages can be taken to reflect the timing of deglaciation of the summit area.

For the Up-valley site (617–615 m asl), three glacially abraded bedrock surfaces give overlapping ^{10}Be surface-exposure ages (9.1 ± 0.4 to 9.8 ± 0.3 ka) (Fig. 4, Table 3). No appropriate boulders were found for comparison with the bedrock samples; however, the internal agreement between the three bedrock surfaces suggests that nuclide inheritance is not a likely issue.

For Lobe 2 (542–538 m asl), three large boulders give overlapping ^{10}Be surface-exposure ages (10.3 ± 0.4 to 10.7 ± 0.4 ka) (Fig. 4, Table 3). For Lobe 3 (528–515 m asl), four large boulders give six ^{10}Be surface-exposure ages (9.6 ± 0.5 to 11.0 ± 0.5 ka) where five of the six ages overlap (Fig. 4, Table 3). Note that two of the boulders (D, F) each have replicate samples with overlapping results.

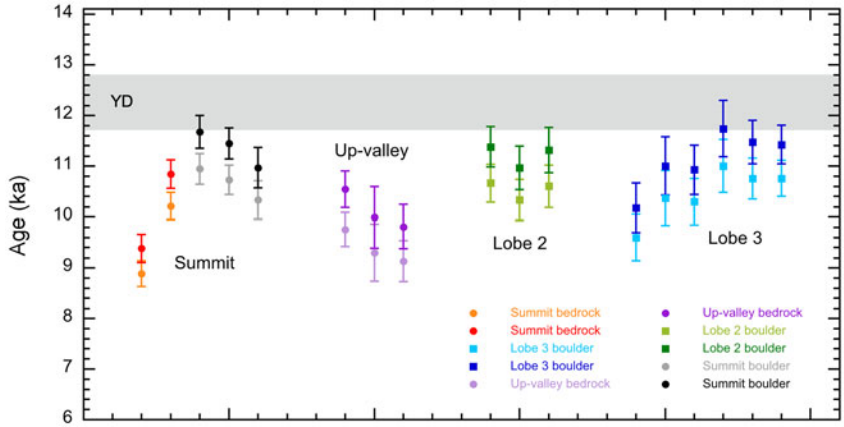

Figure 4. (color online) The distribution of calculated (pale symbols) and corrected/recomputed (dark symbols) ^{10}Be surface-exposure ages for the Summit, Up-valley, Lobe 2, and Lobe 3 sites. Correction was made for erosion (all samples, except ØYB 1309), and for temporal/local changes in ^{10}Be production rate due to glacio-isostatic uplift (all samples), snow cover (all samples), and vegetation (Up-valley only). The total impact of all quantifiable ages is in the order of a 6%–8% increase. The order of samples for individual sites follows the sample labelling (Table 1). Error bars show the 1σ analytical uncertainty. Gray band marks the time interval of the Younger Dryas stadial.

Relevant correction factors and corrected ^{10}Be ages

It is unlikely that the dated rock surfaces are unaffected by processes occurring since the timing of initial exposure. In this study, we consider chemical weathering to be a relevant prerequisite for erosion at all sites. Moreover, changing atmospheric depth caused by uplift (glacio-isostatic rebound) and seasonal snow cover are relevant for all sites, whereas temporal shielding by vegetation is relevant only for the Up-valley site. The relevant correction factors are described and discussed in the Supplementary material and summarized in Table 2. Based on our observations of the protruding quartz vein in the area, a locally derived erosion rate of 0.48 mm ka^{-1} (i.e., 5 mm in 10.5 ka) has been applied to all samples, except sample ØYB 1309 since this was pure quartz with an unknown erosion rate (and probably episodic loss of grains rather than steady state). The impact of erosion translates to an increase in age of less than 0.5% (i.e., c. 50 years). The maximum uplift correction for the 12–0 ka interval amounts to 4.1% for the Summit site, 4.4% for the Up-valley site, and 4.6% for Lobes 2 and 3. Assuming a moderate snow cover from modern data amounts to reductions in ^{10}Be production of about 1.5% for the Up-valley and Lobe sites and 2.0% for the Summit site. Forest shielding at the Up-valley site for the c. 9.5–0 ka interval results in an average reduction in ^{10}Be production of about 2%.

Recomputed data (i.e., corrected ^{10}Be ages) are presented in the right-most column in Table 3. The corrected ages are first used to assess the inter-site correspondence considering the 1σ analytical uncertainties only (in parentheses). The corrected ^{10}Be ages span from 9.4 ± 0.3 to 11.7 ± 0.6 ka (1σ analytic uncertainty). The total impact of all quantifiable corrections is in the order of 6%–8% (i.e., c. 0.6–0.8 ka). Figure 4 compares the calculated and recomputed (corrected) ages and shows close to insignificant intra-site variation for all four sites: Summit, Up-valley, Lobe 2, and Lobe 3 (Fig. 4, Table 3).

Corrected ^{10}Be surface-exposure ages from the Summit site range from 9.4 ± 0.3 to 11.7 ± 0.3 ka, which overlap within 1σ (Fig. 4, Table 3), except for one obvious outlier (9.4 ± 0.3 ka, ØYB 1301 bedrock). This bedrock sample was collected 1 m from the boulder giving the oldest age at the Summit (11.7 ± 0.3 ka, ØYB 1302). All the other boulder and bedrock samples could have some degree of inheritance, except for the young outlier (ØYB 1301). For this specific setting, however, we suggest that the young bedrock surface age is too young because of temporary debris cover; summit sites with cairns have a high risk of human impact (e.g., cobble removal and quarrying, in connection with cairn-building). The bedrock outcrop has several boulders and cobbles, and the distance to thin till cover is about 1 m. The arithmetic average corrected age with one standard deviation is 11.2 ± 0.4 ka for the Summit site (Table 3).

Corrected ^{10}Be surface-exposure ages from the Up-valley site range from 9.8 ± 0.4 to 10.6 ± 0.4 ka (Fig. 4, Table 3). The Up-valley site shows younger ages than the other sites (Fig. 4), indicating that relevant shielding effects might be unaccounted for, such as prolonged snow cover and/or denser snow in the forest. The arithmetic average corrected age with one standard deviation is 10.1 ± 0.4 ka for the Up-valley site (Table 3).

Corrected ^{10}Be surface-exposure ages from the Lobe 2 site range from 11.0 ± 0.4 to 11.4 ± 0.4 ka (Fig. 4, Table 3), giving an arithmetic average corrected age of 11.2 ± 0.2 ka for Lobe 2. Corrected ^{10}Be surface-exposure ages from the Lobe 3 site range from 10.2 ± 0.5 to 11.7 ± 0.6 ka (Fig. 4, Table 3). The near-outlier age (10.2 ± 0.5 ka, ØYB 1204) overlaps with the other age (ØYB 1205) obtained from the same boulder. The ØYB 1204 sample was detached from the boulder surface via weathered cracks, indicating a higher erosion rate affected by more than one weathering front, possibly standing water and/or former vegetation cover. As there is an intra-boulder correspondence between the two samples

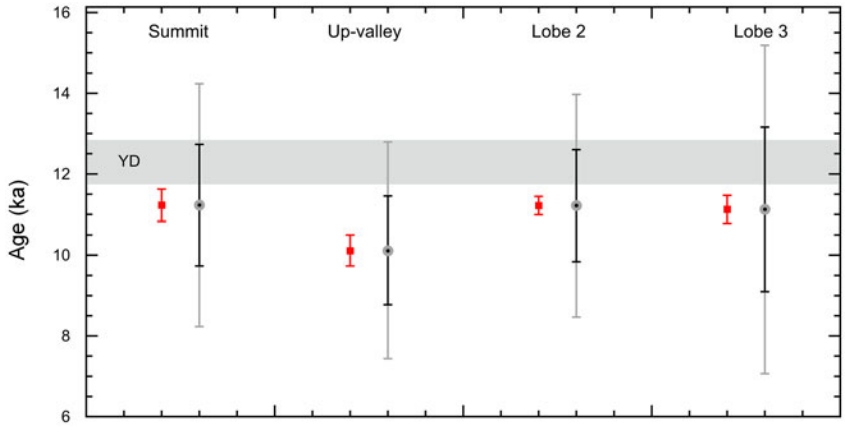

Figure 5. (color online) Average corrected ^{10}Be ages (ka) with one standard deviation (squares) and propagated systematic 1σ and 2σ uncertainties (circles) for each site (see Table 3). Gray band marks the time interval of the Younger Dryas stadial.

from boulder D (Fig. 3), and overlap within 2σ, we include sample ØYB 1204 in the average age. This gives an arithmetic average corrected age of 11.1 ± 0.6 ka for Lobe 3.

The rock-glacier boulders are not expected to have undergone substantial erosion during the downslope creep of the rock glacier, as they are as angular as boulders in the present-day talus slope. Nevertheless, we do not expect nuclide inheritance stemming from the material's pre-rock-glacier history. The large number of boulders constituting the current talus slope and the lobes indicate that there was a high production of talus boulders from the cliff face at some point in time, and/or that boulders were shielded by talus material prior to lobe formation. The very uniform ^{10}Be ages indicate rapid formation of the lobes.

Average corrected ages only comprise ages overlapping within 2σ analytical uncertainties. Only sample ØYB 1301 gives an age that does not overlap with neighboring results within the 2σ uncertainty. Average corrected ages are furthermore presented in two ways: (1) as arithmetic average ages with one–standard deviation uncertainties for assessing inter-site correspondence, and (2) as arithmetic average ages with propagated 1σ analytic (parentheses) and systematic uncertainties for comparing the average corrected ^{10}Be ages with dating results from other techniques.

The inter-site comparison shows very uniform face values for arithmetic average corrected ages (Fig. 5). The crucial point for assessing inter-site correspondence is the uncertainty of the average corrected age. The use of one standard deviations provides a measure of the scatter of the average corrected ages. The smaller uncertainties, compared to the propagated 1σ uncertainties, could allow for a clearer site separation. However, using the standard deviation instead ignores uncertainties associated with the individual ages.

DISCUSSION

Timing of onset and deactivation of rock-glacier activity

According to the average recomputed ^{10}Be ages with one–standard deviation uncertainties (right column, Table 3), the Summit site was deglaciated at 11.2 ± 0.4 ka and the Up-valley site at 10.1 ± 0.4 ka. Of the relict rock-glacier lobes, Lobe 2 has been stable for the past 11.2 ± 0.2 ka and Lobe 3 for 11.1 ± 0.6 ka. The timing of deglaciation represents the maximum age for the inception of rock-glacier activity, whereas the ^{10}Be ages from rock-glacier boulders represent the timing of inactivation. When active, as well as during the melting phase, boulders on a rock glacier can move and change their exposure geometry.

Rapid deglaciation and lobe formation are indicated by the similar ^{10}Be ages obtained from the Summit site, Lobe 2, and Lobe 3. Rock-glacier movement by creep varies with the mean annual ground surface temperature, thickness of snow cover (meltwater supply), and the intensity of ground freezing during winter. In the Swiss Alps, modern annual mean surface-velocity rates of rock glaciers are in the order of 0.1 to 3 m yr^{-1} (Delaloye et al., 2010), suggesting that the 100–200-m-long rock-glacier lobes at Øyberget could have expanded to their present size in less than 100 years. This suggests that there was sufficient time for rock-glacier formation during the deglaciation; the question of whether the environmental conditions during the deglaciation were conducive to rock-glacier formation remains (see further discussion below).

Comparison of ^{10}Be and Schmidt-hammer surface-exposure ages

Schmidt-hammer surface-exposure dating uses rebound (R) values from surfaces of known age for age calibration of R values from surfaces of unknown age (e.g., Shakesby et al., 2011; Wilson and Matthews, 2016). The R value is a measure of the compressive strength of a rock surface, which is reduced with time as a result of chemical weathering. However, aspects of this dating technique require brief clarification in the present context.

An important assumption made by Matthews and colleagues (2013) for converting R values into surface-exposure ages was that the weathering rate is linear with time and hence that two surfaces of known age could be used to derive a

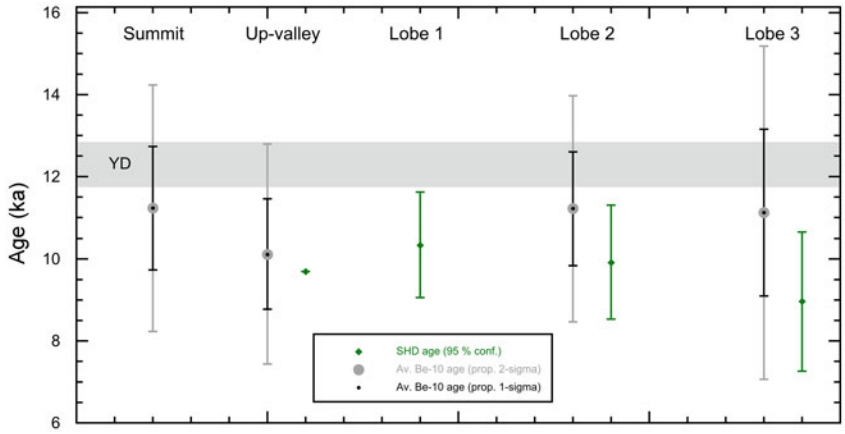

Figure 6. (color online) Comparison between average corrected ^{10}Be surface-exposure ages and Schmidt-hammer surface-exposure (SHD) ages from Matthews et al. (2013). The arithmetic average corrected ^{10}Be ages (circles) are shown with propagated systematic 1σ and 2σ uncertainties. The Schmidt-hammer exposure ages (diamonds) from Matthews et al. (2013) are reported at the 95% confidence interval. Gray band marks the time interval of the Younger Dryas stadial.

linear calibration equation for dating the Øyberget rock glaciers using Schmidt-hammer surface-exposure dating. Matthews and colleagues (2018) further supported this assumption based on the slow rate of chemical weathering of crystalline rock over the relatively short Holocene timescale, especially in arctic-alpine environments (Colman, 1981; Colman and Dethier, 1986; André, 2002; Nicolson, 2008). Particularly pertinent is the test of the linearity assumption by Shakesby and colleagues (2011), who sampled a large number of Holocene raised beaches of known age and showed no improvement in the relationship between R value and time using a non-linear function. Matthews and colleagues (2018) concluded, on this basis and that of Tomkins and colleagues (2016, 2018), that a linear relationship may be applicable for timescales up to c. 20 ka.

Matthews and colleagues (2013) dated the relict talus-derived rock-glacier Lobes 1–3 and obtained ages (± 95% confidence intervals) of 10.3 ± 1.3, 9.9 ± 1.4, and 9.0 ± 1.7 ka, respectively (Fig. 6). The apparent trend of decreasing nominal values with decreasing elevation is, however, not a true trend when the uncertainties are taken into account. All three rock-glacier lobes give R values indicating that they have existed for approximately the same duration of time as the older surface of known age used by Matthews and colleagues (2013), which lies close to our Up-valley site. According to the Schmidt-hammer surface-exposure ages ± 95% confidence intervals, Lobes 1–3 formed between 7.3 and 11.6 ka ago, hence overlapping with the regional deglaciation date of c. 9.7 ka (Dahl et al. 2002).

Comparing the arithmetic average corrected ^{10}Be surface-exposure ages (± systematic 1σ and 2σ uncertainties) from this study (Fig. 6), shows good agreement with the Schmidt-hammer exposure ages of Matthews and colleagues (2013). Figure 6 also indicates that the face value of the ^{10}Be surface-exposure ages may be higher than for the Schmidt-hammer exposure ages. Results from both methods, however, indicate that Lobes 2 and 3 are older than surfaces at the Up-valley site. This warrants further discussion in order to determine whether this is an effect of local environmental conditions affecting both methods (see next paragraph) or reflects details of glacier extent at the end of the deglaciation (see the "Regional implications" section of the Discussion).

The Up-valley site may be affected by slightly different environmental factors than Lobes 1–3. For example, the microclimate in the forest may compromise the assumption of identical weathering rates since forests can have more humid environments than exposed locations because of the shading effect of trees, plant respiration, and the trapping of snow. More humid conditions can enhance the chemical and biological processes associated with chemical weathering, effects not experienced on the forest-free lobes or at the Summit site. Moreover, temporal and spatial variation in plant litter, vegetation, and soil may impact the weathering rate. A slightly higher rate of chemical weathering, at the Up-valley site for example, would also be relevant to the ^{10}Be surface-exposure ages, since this could imply a higher rate of weathering and erosion (i.e., loss of quartz with ^{10}Be, resulting in underestimated ^{10}Be surface-exposure ages).

The most important methodological implications of this comparison between the two dating techniques stem, however, from the similarity of the respective age estimates. Mutual corroboration of the results justifies the very different underlying assumptions of both techniques. Furthermore, the results suggest that the two techniques can be complementary approaches to exposure-age dating, and that greater use could be made of the two techniques together in future research projects involving rock surfaces. The techniques may be particularly compatible on relatively short late Pleistocene and Holocene timescales, where they overlap in their temporal ranges and advantage can be taken of their different practical constraints in terms of cost, time, and technical sophistication. For instance, for lateral moraines with additional boulders from rock falls, it would be a great advantage to apply initial Schmidt-hammer screening when selecting boulder

surfaces to be sampled for cosmogenic nuclide surface-exposure dating.

Environmental conditions for rock-glacier formation

Formation of talus-derived rock glaciers (sensu Barsch, 1996) requires periglacial conditions with permafrost. For the mode of origin of the lobes beneath the south-facing wall of Øyberget, Matthews and colleagues (2013) suggested three hypotheses: (1) that the landforms are produced by (Holocene) major rock-slope failures, (2) paraglacial formation of rock glaciers in the early Holocene, and (3) periglacial rock-glacier formation during an earlier interstadial followed by subsequent survival beneath a cold-based ice sheet. Rockslides or rock avalanches can form coarse debris accumulations (e.g., Ballantyne et al., 2009, 2014; Hermanns et al., 2017), but these will lack morphological features produced by creep of interstitial ice. Several arguments were listed by Matthews and colleagues (2013) against formation entirely by rock-slope failure for the lobes of Øybergsurdi: lack of matching scars on the rock wall, relatively uniform boulder size, small-scale lobate extension relative to potential run-out distance, general integrity of each lobe, and the form of the transverse ridges.

According to the average corrected ^{10}Be surface-exposure ages (± propagated 1σ uncertainties) in this study, summit deglaciation (11.2 ± 0.7 ka) and stabilization of rock-glacier lobes (Lobe 2: 11.2 ± 0.7 ka; Lobe 3: 11.1 ± 1.2 ka), occurred faster than our data can resolve; therefore, both the inception and cessation of rock-glacier activity occurred very early after, or even during, the deglaciation. In the "Timing of onset and deactivation" section of the Discussion, we argued that modern data indicate that lobes of this size can form in less than 100 years, given favorable environmental conditions of permafrost and debris supply.

Permafrost at the location of the lobes is unlikely based on the present-day distribution of permafrost in southern Norway and the work of Lilleøren and colleagues (2012) in particular. Using thermal properties from two boreholes at Jetta, 60 km east down-valley of Øyberget, the authors modelled ground temperatures over the Holocene time interval. Permafrost is recorded today at 1560 m asl (borehole JetBH1), but not at 1218 m asl (borehole JetBH3). The initial model domain of Lilleøren and colleagues (2012) contains no permafrost because of lack of information about the subglacial temperatures of the last ice-sheet cover, and the model outputs are thus minimum estimates. Temperatures below 0°C are demonstrated for the 1560-m borehole site in the early and late Holocene, but temperatures remained above 0°C for the whole Holocene at the 1218-m borehole site. A permafrost environment below 1200 m asl for the early Holocene in Ottadalen is therefore incompatible with the simulated borehole data, and it can be confidently predicted that no permafrost existed at the elevation of the rock-glacier lobes at the foot of Øyberget.

Another possibility for formation under a conventional periglacial environment would be during the Ålesund interstadial (38.2–34.5 ka, Mangerud et al., 2011), the latest period of ice-free conditions before the Holocene. As discussed by Matthews and colleagues (2013), this implies preservation of the rock-glacier lobes underneath cold-based ice. Evidence of the former existence of cold-based ice, such as till deposits overlying glacio-fluvial or glacio-lacustrine sediments, is found close by (Bergersen and Garnes, 1983), although the timing of ice-free conditions in upper Ottadalen has not been confirmed by empirical dating. Assuming a complex exposure history for Lobes 2 and 3 with c. 3 ka of exposure (37–34 ka, i.e., the Ålesund interstadial), c. 23 ka of burial (34–11 ka, glacial build-up to LGM and subsequent persistence), and c. 11 ka (the Holocene) of exposure, and applying the same corrections for the Holocene, an apparent minimum ^{10}Be surface-exposure age of about 13 ka would be expected. The present ^{10}Be dataset has 1σ uncertainties ranging from 2.6% to 6.0%, so the ages of surfaces with a brief pre-exposure and long burial history could still overlap within 1σ or 2σ. Taken at face value, cosmogenic nuclide surface-exposure dating cannot reject the hypothesis of preservation beneath a cold-based ice sheet. The agreement between ^{10}Be surface-exposure ages from bedrock and boulders at the Summit, however, argues against a pre-Holocene, subglacial preservation history of the rock-glacier lobes.

With rejection of the rock-slope failure hypothesis, the absence of an early Holocene permafrost environment, and with intra- and inter-site agreement of ^{10}Be ages making pre-Holocene exposure unlikely, we are left with two possible explanations for the ^{10}Be dataset: (1) the paraglacial hypothesis, or (2) both sets of ^{10}Be and Schmidt-hammer surface-exposure ages are incorrect.

Formation of rock-glacier lobes in the absence of permafrost under paraglacial conditions would require burial of residual glacial ice in the valley by a rapid and large debris supply (without major rock-slope failure and associated major rock-avalanche scars) and subsequent creep of the debris-covered ice. A paraglacial origin is in general supported by an increasing number of observations in the region. In Storfjorden, 50 km west of Øyberget, for example, Longva and colleagues (2009) found that rock-avalanche frequency was very high during YD and Preboreal times. A rock-avalanche deposit in Innerdalen (62.72°N, 8.73°E) has been shown to have been formed when there was still ice in the valley (Schleier et al., 2015), despite the low preservation potential of such deposits. Most dated rock-avalanche deposits, however, lag the deglaciation by 1–2 ka. Hermanns and colleagues (2017) show this by comparing a compilation of ^{10}Be surface-exposure ages of rock-avalanche deposits and scars with the ice-sheet retreat chronology in southern and western Norway. Rapid supply of large quantities of debris in the early Holocene can be attributed to the mechanical instability/weakness of newly exposed landscapes (e.g., Ellis and Calkin, 1984; Blikra and Nemec, 1998). The lack of large scars or indentations and the steepness of the cliff face at Øyberget can be explained, along with the large size of

boulders in the lobes and talus, by bedrock properties. In the roadcut near the Up-valley site, the exposed bedrock shows complex banding of variable thickness (< 3 m) and composition that dip 30–60° north, suggesting that the southern face of the Øyberget should be relatively stable as the angle of dip does not favor sliding from north to south.

Regional implications of the ^{10}Be surface-exposure ages from Øyberget

Vertical down-wastage of the last ice sheet in this region makes the apparent ^{10}Be age relationship between Summit and Up-valley sites reasonable. It is, however, problematic that the Up-valley site provides significantly younger ages than the Lobes. This situation could be explained if the Up-valley site has experienced additional shielding than has been accounted for. This is considered unlikely as the same relative age pattern is revealed by the Schmidt-hammer surface-exposure ages. Increased weathering would be evident from the R values and cannot be the explanation. Only a later deglaciation time or a post-deglaciation erosional event could explain the agreement between the two methods. Hence, this relatively young age may be accounted for by a deglaciation model involving vertical down-wastage followed by up-valley retreat of a trunk glacier in upper Ottadalen.

In the DATED-1 reconstruction of Hughes and colleagues (2016), the time-slice reconstructions suggest that deglaciation of upper Ottadalen occurred around 11–10 ka; Øyberget is outside the minimum extent of the SIS at this time but inside the maximum extent. Our data indicate that their boundary for the most-credible SIS extent at 11 ka should be moved east of the Øyberget study area.

The average corrected deglaciation age for the deglaciation of the summit of Øyberget at 11.2 ± (0.7) 1.5 ka (Table 3), is in agreement with the youngest boulder age of 10.9 ± 2.6 ka 60 km down valley (our recalculation from data reported by Goehring et al., 2008). The timing of valley deglaciation may therefore have been slightly earlier than suggested by the aforementioned ice-sheet reconstruction. The indistinguishable ages from similar elevations, although 60 km apart, is in agreement with the reconstructed course of the deglaciation by Garnes and Bergersen (1980), where the ice sheet underwent vertical down-wasting after a final phase of ice movement towards the northeast. During the down-wasting, Ottadalen was situated between the main water divide in the north and the ice-divide in the south, and the ice-sheet surface is believed to have had a relatively small gradient (c. 10 m km^{-1}) based on lateral, erosional, and accumulation meltwater features in this area, in particular when the ice surface came down to about 1200 m asl (Garnes and Bergersen, 1980). This may have resulted in dynamically active ice at the Up-valley site and stagnant, dynamically inactive ice in lower-elevation areas (i.e., valley bottoms). Temporal and spatial complexities associated with vertical down-wasting of the last ice sheet makes reconstruction of the last deglaciation in such regions particularly challenging. However, new geochronologic tools and refined numerical models are expected to disentangle information on the final demise of large ice sheets.

CONCLUSIONS

The purpose of this study was to evaluate the timing and environmental controls on past rock-glacier formation in southern Norway. To do this, we first wanted to test whether boulders on relict rock-glacier lobes at Øyberget could be reliably dated with in situ ^{10}Be, and if so, to compare the results with previously published Schmidt-hammer surface-exposure ages. Age determination is crucial to obtaining further information about the environmental conditions under which the rock-glacier lobes were formed. The study has reached several conclusions where average corrected ^{10}Be ages are given in ka with propagated 1σ (analytic) and systematic uncertainties. Relict rock-glacier lobes in southern Norway can be reliably dated with in situ ^{10}Be, judging from the uniform data obtained from two examples at Øyberget in upper Ottadalen. Rock-glacier Lobes 2 and 3 at the foot of Øyberget became inactive around 11.2 ± (0.7) 1.4 and 11.1 ± (1.2) 2.3 ka, respectively, when corrected for glacio-isostatic uplift, snow shielding, and erosion. The ages are slightly older than, but not statistically different from, previously published Schmidt-hammer surface-exposure ages from the same rock-glacier lobes. The close similarity corroborates the results of both dating techniques and supports their mutual compatibility and complementarity. According to the ^{10}Be data, the Summit (1225–1175 m asl) of Øyberget was deglaciated around 11.2 ± (0.7) 1.5 ka, when glacio-isostatic rebound, snow shielding, and erosion are taken into account. There is no evidence for any nuclide inheritance effect. The Up-valley site from Øyberget has been ice free for the last 10.1 ± (0.8) 1.3 ka when glacio-isostatic rebound, snow shielding, and erosion are taken into account. This justifies the previously assumed deglaciation date of c. 9.7 ka used for Schmidt-hammer surface-exposure dating. The uniformity of the ^{10}Be surface-exposure ages from all four sites leads to rejection of the hypothesis that the rock-glacier lobes could have been preserved beneath a cold-based, low-erosive glacier during the LGM. As the timing of formation of the rock-glacier lobes is incompatible with the non-permafrost climatic conditions that existed at the sites in the early Holocene, their formation is explained as a result of rapid paraglacial formation involving enhanced debris supply and burial of residual ice immediately after deglaciation. The results demonstrate that rock-glacier lobes may form over a relatively short period of time (hundreds rather than thousands of years) under non-permafrost conditions and arguably exemplify a paraglacial mode of formation.

ACKNOWLEDGMENTS

Henriette Linge thanks Hanne Linge for crushing and mineral separation of the rock samples, Lars Evje and Maria Miguens-Rodriguez for assistance during laboratory processing of the samples, and

Stein-Erik Lauritzen and Aage Paus for data discussions. The 2013 samples were collected during the Swansea University Jotunheimen Research Expedition 2013, and this paper represents Jotunheimen Research Expeditions Contribution No. 212. Sample preparation and AMS analysis for in situ cosmogenic ^{10}Be surface-exposure dating was funded by the Bjerknes Centre for Climate Research. We thank two anonymous reviewers for providing detailed and constructive comments on an earlier version of this manuscript. The manuscript further benefitted from the comments given by Attila Çiner, an anonymous reviewer, and *Quaternary Research* Associate Editor Jim O'Connor.

SUPPLEMENTARY MATERIAL

To view supplementary material for this article, please visit https://doi.org/10.1017/qua.2020.10.

REFERENCES

Andersen, B.G., Lundqvist, J., Saarnisto, M., 1995. The Younger Dryas margin of the Scandinavian Ice Sheet—An introduction. *Quaternary International* 28, 145–146.

Andersen, J.L., Egholm, D.L., Knudsen, M.F., Linge, H., Jansen, J.D., Goodfellow, B.W., Pedersen, V.K., Tikhomirov, D., Olsen, J., Fredin, O., 2019. Pleistocene evolution of a Scandinavian plateau landscape. *Journal of Geophysical Research: Earth Surface* 123, https://doi.org/10.1029/2018JF004670.

André, M.F., 1994. Rock glaciers in Svalbard. *Geografiska Annaler: Series A, Physical Geography* 76, 235–245.

André, M.F., 2002. Rates of postglacial rock weathering on glacially scoured outcrops (Abisko -Riksgränsen area, 68°N). *Geografiska Annaler* 84A, 139–150.

Balco, G., 2017. Documentation v3 exposure age calculator (accessed September 2018). https://sites.google.com/a/bgc.org/v3docs/.

Balco, G., Stone, J.O., Lifton, N.A., Dunai, T.J., 2008. A complete and easily accessible means of calculating surface exposure ages or erosion rates from ^{10}Be and ^{26}Al measurements. *Quaternary Geochronology* 3, 174–195.

Ballantyne, C.K., Schnabel, C., Xu, S., 2009. Exposure dating and reinterpretation of coarse debris accumulations ('rock glaciers') in the Cairngorm Mountains, Scotland. *Journal of Quaternary Science* 24, 19–31.

Ballantyne, C.K., Wilson, P., Gheorghiu, D., Rodés, À., 2014. Enhanced rock-slope failure following ice-sheet deglaciation: timing and causes. *Earth Surface Processes and Landforms* 39, 900–913.

Barsch, D., 1996. *Rockglaciers*. Springer, Berlin.

Bergersen, O.F., Garnes, K., 1983. Glacial deposits in the culmination zone of the Scandinavian ice sheet. Ehlers, J., (ed.), *Glacial deposits in north-west Europe*, 29–40, A.A. Balkema, Rotterdam.

Berthling, I., 2011. Beyond confusion: Rock glaciers as cryo-conditioned landforms. *Geomorphology* 131, 98–106.

Berthling, I., Etzelmüller, B., 2007. Holocene rockwall retreat and the estimation of rock glacier age, Prins Karls Forland, Svalbard. *Geografiska Annaler: Series A, Physical Geography* 89, 83–93.

Blikra, L.H., Nemec, W., 1998. Postglacial colluvium in western Norway: depositional processes, facies and palaeoclimatic record. *Sedimentology* 45, 909–959.

Çiner, A., Sarikaya, M.A., Yildirim, C., 2017. Misleading old age on a young landform? The dilemma of cosmogenic inheritance in surface exposure dating: moraines vs. rock glaciers. *Quaternary Geochronology* 42, 76–88.

Child, D., Elliott, G., Mifsud, C., Smith, A.M., Fink, D., 2000. Sample processing for earth science studies at ANTARES. *Nuclear Instruments and Methods in Physics Research* Section B 172, 856–860.

Colman, S.M., 1981. Rock-weathering rates as functions of time. *Quaternary Research* 15, 250–264.

Colman, S.M., Dethier, D.P. (Eds.), 1986. *Rates of chemical weathering of rocks and minerals*. 1st edition, Academic Press, London.

Cossart, E., Fort, M., Bourlès, D., Carcaillet, J., Perrier, R., Siame, L., Braucher, R., 2010. Climatic significance of glacier retreat and rockglaciers re-assessed in the light of cosmogenic dating and weathering rind thickness in Clarée valley (Briançonnais, French Alps). *Catena* 80, 204–219.

Dahl, S.O., Nesje, A., Lie, Ø., Fjordheim, K., Matthews, J.A., 2002. Timing, equilibrium-line altitudes and climatic implications of two early-Holocene glacier readvances during the Erdalen Event at Jostedalsbreen, western Norway. *The Holocene* 12, 17–25.

Dehls, J.F., Olesen, O., Olsen, L., Blikra, L.H., 2000. Neotectonic faulting in northern Norway: the Stuoragurra and Nordmannvikdalen postglacial faults. *Quaternary Science Reviews* 19, 1447–1460.

Delaloye, R., Lambiel, C., Gärter-Roer, I., 2010. Overview of rock glacier kinematics research in the Swiss Alps. *Geographica Helvetica* 65, 135–145.

Dunne, J., Elmore, D., Muzikar, P., 1999. Scaling factors for the rates of production of cosmogenic nuclides for geometric shielding and attenuation at depth on sloped surfaces. *Geomorphology* 27, 3–11.

Ellis, J.M., Calkin, P.E., 1984. Chronology of Holocene glaciation, Central Brooks Range, Alaska. *Geological Society of America Bulletin* 95, 897–912.

Engel, Z. 2007. Measurement and age assignment of intact rock strength in the Krkonoše Mountains, Czech Republic. *Zeitschrift für Geomorphologie* 51, 69–80.

Fuchs, M.C., Böhlert, R., Krbetschek, M., Preusser, F., Egli, M., 2013. Exploring the potential of luminescence methods for dating Alpine rock glaciers. *Quaternary Geochronology* 18, 17–33.

Garnes, K., Bergersen, O.F., 1980. Wastage features of the inland ice sheet in central South-Norway. *Boreas* 9, 251–269.

Goehring, B.M., Brook, E.J., Linge, H., Raisbeck, G.M., Yiou, F., 2008. Beryllium-10 exposure ages of erratic boulders in southern Norway and implications for the history of the Fennoscandian Ice Sheet. *Quaternary Science Reviews* 27, 320–336.

Gosse, J.C., Phillips, F.M., 2001. Terrestrial in situ cosmogenic nuclides: theory and application. *Quaternary Science Reviews* 20, 1475–1560.

Haeberli, W., Kääb, A., Wagner, S., Mühll, D.V., Geissler, P., Haas, J.N., Glatzel-Mattheier, H., Wagenbach, D., 1999. Pollen analysis and ^{14}C age of moss remains in a permafrost core recovered from the active rock glacier Murtèl-Corvatsch, Swiss Alps: geomorphological and glaciological implications. *Journal of Glaciology* 45, 1–8.

Hermanns, R.L., Schleier, M., Böhme, M., Blikra, L.H., Gosse, J., Ivy-Ochs, S., Hilger, P., 2017. Rock-avalanche activity in W and S Norway peaks after the retreat of the Scandinavian Ice Sheet. In: Mikoš M., Vilímek V., Yin Y., Sassa K. (eds.), *Advancing Culture of Living with Landslides, Volume 5 Landslides in Different Environments*. WLF 2017. Springer. DOI 10.1007/978-3-319-53483-1_39.

Hippolyte, J.-C., Bourlès, D.L., Braucher, R., Carcaillet, J., Léanni, L., Arnold, M., Aumaitre, G., 2009. Cosmogenic ^{10}Be dating of a sackung and its faulted rock glaciers, in the Alps of Savoy. *Geomorphology* 108, 312–320.

Høydedata. 2018. Free access to digital elevation model of Norway (incomplete coverage) (accessed September 2018). https://hoydedata.no/LaserInnsyn/.

Hughes, A.L.C., Gyllencreutz, R., Lohne, Ø.S., Mangerud, J., Svendsen, J.I., 2016. The last Eurasian ice sheets—a chronological database and time-slice reconstruction, DATED-1. *Boreas* 45, 1–45.

Humlum, O., 2000. The geomorphic significance of rock glaciers: estimates of rock glacier debris volumes and headwall recession rates in West Greenland. *Geomorphology* 35, 41–67.

Ivy-Ochs, S., Kerschner, H., Schlüchter, C., 2007. Cosmogenic nuclides and the dating of Lateglacial and Early Holocene glacier variations: The Alpine persective. *Quaternary International* 164–165, 53–63.

Kääb, A., 2013. Rock glaciers and protalus forms. In Elias, S.A. (Ed.), *Encyclopedia of Quaternary Science*, 2nd Edition. Elsevier, Amsterdam.

Kellerer-Pirklbauer, A., Wangensteen, B., Farbrot, H., Etzelmüller, B., 2008. Relative surface age-dating of rock glacier systems near Hólar in Hjaltadalur, northern Iceland. *Journal of Quaternary Science* 23, 137–151.

Knight, J., Harrison, S., Jones, D.B., 2019. Rock glaciers and the geomorphological evolution of deglacierizing mountains. *Geomorphology* 324, 14–24.

Kohl, C.P., Nishiizumi, K., 1992. Chemical isolation of quartz for measurement of in-situ-produced cosmogenic nuclides. *Geochimica et Cosmochimica Acta* 56, 3538–3587.

Konrad, S.K., Humphrey, N.F., Steig, E.J., Clark, D.H., Potter, N. Jr., Pfeffer, W.T., 1999. Rock glacier dynamics and paleoclimatic implications. *Geology* 27, 1131–1134.

Lal, D., 1991. Cosmic ray labeling of erosion surfaces: *in situ* nuclide production rates and erosion models. *Earth and Planetary Science Letters* 104, 424–439.

Lifton, N., 2016. Implications of two Holocene time-dependent geomagnetic models for cosmogenic nuclide production rate scaling. *Earth and Planetary Science Letters* 433, 257–268.

Lilleøren, K.S., Etzelmüller, B., 2011. A regional inventory of rock glaciers and ice-cored moraines in Norway. *Geografiska Annaler: Series A, Physical Geography* 93, 175–191.

Lilleøren, K.S., Etzelmüller, B., Schuler, T.V., Gisnås, K., Humlum, O., 2012. The relative age of mountain permafrost—estimation of Holocene permafrost limits in Norway. *Global and Planetary Change* 92–93, 209–223.

Longva, O., Blikra, L.H., Dehls, J.F., 2009. Rock avalanches – distribution and frequencies in the inner part of Storfjorden, Møre og Romsdal County, Norway. *Geological Survey of Norway Report* No. 2009.002. http://www.ngu.no/upload/Publikasjoner/Rapporter/2009/2009_002.pdf.

Lutro, O., Tveten, E., 1996. Geologisk kart over Norge, berggrunnskart Årdal M 1:250.000. Noregs geologiske undersøking, Trondheim. https://www.ngu.no/upload/Publikasjoner/Kart/B250/Aardal.pdf

Lysså, A., Knies, J., Larsen, E., 2008. Kunnskap om istider og landformer—nøkkelen til forståelsen av klimavariasjoner. *Gråsteinen* 12, 41–57.

Mangerud, J., Gyllencreutz, R., Lohne, Ø., Svendsen, J.I., 2011. Glacial history of Norway. In: Ehlers, J., Gibbard, P.L., Hughes, P.D., (Eds.), *Quaternary Glaciations—Extent and Chronology —A Closer Look*, Elsevier, Amsterdam, pp. 279–298.

Marr, P., Winkler, S., Binnie, S.A., Löffler, J., 2019. 10Be-based exploration of the timing of deglaciation in two selected areas of southern Norway. *E&G Quaternary Science Journal* 68, 165–176.

Matthews, J.A., Nesje, A., Linge, H., 2013. Relict talus-foot rock glaciers at Øyberget, Upper Ottadalen, southern Norway: Schmidt hammer exposure ages and palaeoenvironmental implications. *Permafrost and Periglacial Processes* 24, 336–346.

Matthews, J.A., Winkler, S., Wilson, P., Tomkins, M.D., Dortch, J.M., Mourne, R.W., Hill, J.L., Owen, G., Vater, A.E., 2018. Small rock-slope failures conditioned by Holocene permafrost degradation: a new approach and conceptual model based on Schmidt-hammer exposure-age dating, Jotunheimen, southern Norway. *Boreas* 47, 1144–1169.

Nesje, A., 2009. Latest Pleistocene and Holocene alpine glacier fluctuations in Scandinavia. *Quaternary Science Reviews* 28, 2119–2136.

Nicholson, D.T., 2008. Rock control on microweathering of bedrock surfaces in a periglacial environment. *Geomorphology,* 101, 655–665.

NORPERM. 2018. Permafrost: Norwegian mainland. Free access to information on ground temperatures provided by the permafrost database (accessed September 2018). http://geo.ngu.no/kart/permafrost/?lang=English.

Paasche, Ø., Dahl, S.O., Løvlie, R., Bakke, J., Nesje, A., 2007. Rockglacier activity during the Last Glacial-Interglacial transition and Holocene spring snowmelting. *Quaternary Science Reviews* 26, 793–807.

Paus, A., 2010. Vegetation and environment of the Rødalen alpine area, Central Norway, with emphasis on the early Holocene. *Vegetation History and Archaeobotany* 19, 29–51.

Paus, A., Haugland, V., 2017. Early- to mid-Holocene forest-line and climate dynamics in southern Scandes mountains inferred from contrasting megafossil and pollen data. *The Holocene* 27, 361–383.

Paus, A., Haflidason, H., Routh, J., Naafs, B.D.A., Thoen, M.W., 2019. Environmental responses to the 9.7 and 8.2 cold events at two ecotonal sites in the Dovre mountains, mid-Norway. *Quaternary Science Reviews* 205, 45–61.

Sánchez, J.S., Mosquera, D.F., Romaní, J.R.V., 2009. Assessing the age-weathering correspondence of cosmogenic ^{21}Ne dated Pleistocene surfaces by the Schmidt Hammer. *Earth Surface Processes and Landforms* 34, 1121–1125.

Schleier, M., Hermanns, R.L., Rohn, J., Gosse, J.C., 2015. Diagnostic characteristics and paleodynamics of supraglacial rock avalanches, Innerdalen, western Norway. *Geomorphology* 245, 23–39.

SeNorge. 2018. Free access to daily updated maps of snow, weather and water conditions and climate in Norway (accessed September 2018). http://www.senorge.no.

Shakesby, R.A., Matthews, J.A., Owen, G., 2006. The Schmidt hammer as a relative-age dating tool and its potential for calibrated-age dating in Holocene glaciated environments. *Quaternary Science Reviews* 25, 2846–2867.

Shakesby, R.A., Matthews, J.A., Karlén, W., Los, S.O., 2011. The Schmidt hammer as a Holocene calibrated-age dating technique: Testing the form of the R-value–age relationship and defining the predicted-age errors. *The Holocene* 21, 615–628.

Sohbati, R., Murray, A.S., Chapot, M.S., Jain, M., Pederson, J., 2012. Optically stimulated luminescence (OSL) as a chronometer for surface exposure dating. *Journal of Geophysical Research* 117, B09202, doi:10.1029/2012JB009383.

Stroeven, A.P., Heyman, J., Fabel, D., Björk, S., Caffee, M.W., Fredin, O., Harbor, J.M., 2015. A new Scandinavian reference ^{10}Be production rate. *Quaternary Geochronology* 29, 104–115.

Stroeven, A.P., Hättestrand, C., Kleman, J., Heyman, J., Fabel, D., Fredin, O., Goodfellow, B.W., *et al*., 2016. Deglaciation of Fennoscandia. *Quaternary Science Reviews* 147, 91–121. doi:10.1016/j.quascirev.2015.09.016.

Tomkins, M.D., Dortch, J.M., Hughes, P.D., 2016. Schmidt hammer exposure dating (SHED): Establishment and implications for the retreat of the last British Ice Sheet. *Quaternary Geochronology* 33, 46–60.

Tomkins, M.D., Dortch, J.M., Hughes, P.D., Huck, J.J., Stimson, A.G., Delmas, M., Calvet, M., Pallàs, R., 2018. Rapid age assessment of glacial landforms in the Pyrenees using Schmidt hammer exposure dating (SHED). *Quaternary Research* 90, 26–37.

Xu, S., Dougans, A.B., Freeman, S.P.H.T., Schnabel, C., Wilcken, K.M., 2010. Improved ^{10}Be and ^{26}Al-AMS with a 5 MV spectrometer. *Nuclear Instruments and Methods in Physics Research* B 268, 736–738.

Vorren, T.O., Mangerud, J., Blikra, L.H., Nesje, A., Sveian, H., 2008. The emergence of modern Norway. The last 11,500 years—the Holocene. In: Ramberg, I.B., Bryhni, I., Nøttvedt, A., Rangnes, K. (Eds.). *The Making of a Land—The Geology of Norway*, 534–559, Geological Society of Norway, Trondheim.

Whalley, W.B., Azizi, F., 2003. Rock glaciers and protalus landforms: Analogous forms and ice sources on Earth and Mars. *Journal of Geophysical Research* 108, E4, 8032, doi:10.1029/2002JE001864.

Wilson, P., Matthews, J.A., 2016. Age assessment and implications of late Quaternary periglacial and paraglacial landforms on Muckish Mountain, northwest Ireland, based on Schmidt-hammer exposure-age dating (SHD). *Geomorphology* 270, 134–144.

Wilson, P., Dunlop, P., Millar, C., Wilson, F.A. 2019a. Age determination of glacially-transported boulders in Ireland and Scotland using Schmidt-hammer exposure-age dating (SHD) and terrestrial cosmogenic nuclide (TCN) exposure-age dating. *Quaternary Research*, DOI: https://doi.org/10.1017/qua.2019.12.

Wilson, P., Linge, H., Matthews, J.A., Mourne, R.W., Olsen, J., 2019b. Comparative numerical surface exposure-age dating (^{10}Be and Schmidt hammer) of an early-Holocene rock avalanche at Alstadfjellet, Valldalen, southern Norway. *Geografiska Annaler: Series A, Physical Geography*, https://doi.org/10.1080/04353676.2019.1644815.

Winkler, S., 2009. First attempt to combine terrestrial cosmogenic nuclide (^{10}Be) and Schmidt hammer relative-age dating: Strauchon Glacier, Southern Alps, New Zealand. *Central European Journal of Geosciences* 1, 274–290.